JGR Biogeosciences

RESEARCH ARTICLE
10.1029/2018JG004666

Groundwater-River Water Exchange Enhances Growing Season Evapotranspiration and Carbon Uptake in a Semiarid Riparian Ecosystem

Justine E. C. Missik[1], Heping Liu[1], Zhongming Gao[1], Maoyi Huang[2], Xingyuan Chen[2], Evan Arntzen[2], Douglas P. Mcfarland[2], Huiying Ren[2], P. Scott Titzler[2], Jonathan N. Thomle[2], and Amy Goldman[2]

[1]Laboratory for Atmospheric Research, Department of Civil and Environmental Engineering, Washington State University, Pullman, WA, USA, [2]Pacific Northwest National Laboratory, Richland, WA, USA

Abstract Semiarid ecosystems play a critical role in determining the interannual variability of the global terrestrial carbon sink. Water availability is a critical driver of productivity in semiarid ecosystems, which often alternate between carbon sink/source functioning during wet/dry years. In this study, we investigate how groundwater availability resulting from groundwater-river water exchange influences net ecosystem exchange of CO_2 (NEE), evapotranspiration (ET), and the surface energy balance at two semiarid ecosystems along the Columbia River in central Washington, USA. We examined 1 year of eddy covariance measurements from an upland sagebrush ecosystem primarily fed by rainfall without groundwater access and a riparian grassland ecosystem with groundwater access during the dry season due to lateral groundwater-river water exchange. The two sites had distinct seasonal patterns of NEE and ET, driven by differences in water availability. While NEE at the upland sagebrush site was strongly constrained by water availability during the dry months, access to groundwater allowed the riparian site to maintain high NEE magnitude and ET during the same dry months. The riparian site had larger annual gross primary productivity than the upland site (612 vs. 424 gC/m^2), which was offset by higher ecosystem respiration (558 vs. 363 gC/m^2). Thus, the magnitude of the annual NEE at the upland site was larger than that at the riparian site (−62 vs. −54 gC/m^2). Our results demonstrate that groundwater access determined by connectivity between groundwater and surface water can be a critical driver of carbon uptake and ET in semiarid ecosystems.

Plain Language Summary Semiarid ecosystems play a critical role in determining the interannual variability of the global terrestrial carbon sink. Water availability is a critical factor influencing the productivity of semiarid ecosystems, which often alternate between functioning as carbon sinks during wet years and carbon sources during dry years. In this study, we investigate how groundwater availability resulting from groundwater-river water exchange influences carbon uptake and evapotranspiration at two semiarid ecosystems along the Columbia River corridor in central Washington, USA. We examined 1 year of measurements from an upland sagebrush ecosystem without groundwater access and a riparian grassland ecosystem with access to groundwater during the dry season due to lateral groundwater-river water exchange. The two sites had distinct seasonal patterns of carbon uptake, driven by differences in water availability between the two sites. While carbon uptake at the upland sagebrush site was strongly constrained by water availability during the dry summer months, access to groundwater allowed the riparian site to maintain high carbon uptake and evapotranspiration during the same dry months. Our results demonstrate that groundwater access can be a critical factor influencing carbon uptake and evapotranspiration in semiarid ecosystems.

Key Points:
- The effects of water accessibility on carbon and water cycling in semiarid ecosystems are investigated
- Carbon uptake was strongly constrained by moisture availability during dry months in an upland ecosystem without groundwater access
- Lateral groundwater-river water exchange allowed a riparian semiarid ecosystem to maintain high carbon uptake and evapotranspiration during dry months

Supporting Information:
- Supporting Information S1

Correspondence to:
H. Liu,
heping.liu@wsu.edu

Citation:
Missik, J. E. C., Liu, H., Gao, Z., Huang, M., Chen, X., Arntzen, E., et al. (2019). Groundwater-river water exchange enhances growing season evapotranspiration and carbon uptake in a semiarid riparian ecosystem. *Journal of Geophysical Research: Biogeosciences*, *124*, 99–114. https://doi.org/10.1029/2018JG004666

Received 23 JUN 2018
Accepted 16 DEC 2018
Accepted article online 20 DEC 2018
Published online 12 JAN 2019

1. Introduction

Dryland ecosystems in arid and semiarid climate zones constitute around 40% of Earth's land surface and thus are a major component of Earth's carbon, water, and energy budgets. Investigation of the response of dryland ecosystems to climatic variability is essential for improving our projections of the global carbon and water cycles. Global dryland area is projected to expand considerably under climate change (J. Huang et al., 2015), and recent studies indicate that vegetation productivity in semiarid ecosystems is critically important in determining interannual variability in the global terrestrial carbon sink (Ahlström et al.,

2015; L. Huang et al., 2016; Poulter et al., 2014). Climatic and hydrologic shifts have the potential to significantly impact carbon uptake in dryland ecosystems, as dryland ecosystem productivity is primarily driven by water availability.

Projections indicate that climate change will significantly alter seasonal precipitation and temperature regimes (Leng et al., 2016) and increase the extent and severity of droughts (Dai, 2012; Trenberth et al., 2013). In the Pacific Northwest, summers are projected to become warmer and drier (Mote & Salathé, 2010; Rupp et al., 2017). In addition, climate change will have a significant impact on surface water resources, with more than 40% of the conterminous United States projected to experience significant changes in the distributions of summer and winter runoff by the end of the 21st century (Leng et al., 2016). Changes in precipitation, runoff, and surface water will also impact groundwater recharge and groundwater-surface water interactions (Green et al., 2011; Taylor et al., 2013).

Groundwater resources can be an important source of ecosystem water availability (Miller et al., 2010; Scott et al., 2000; Scott, Cable, Huxman, et al., 2008), and changes in groundwater resources have the potential to significantly alter ecosystem structure and functioning. Changes in groundwater resources may cause shifts in vegetation location and species composition (Kløve et al., 2014). In addition, interactions between vegetation structure and hydrological characteristics play an important role in determining the response of ecosystem functioning to different climate conditions.

Groundwater can enhance ecosystem carbon uptake by providing a stable water source that allows ecosystems to maintain high transpiration and productivity during dry periods (Miller et al., 2010; Scott et al., 2014). A continental-scale study of the major river basins in North America found that including lateral groundwater flows in a coupled land surface-subsurface model increased the fraction of transpiration to total evapotranspiration (ET) from 47 ± 13% to 62 ± 12% (Maxwell & Condon, 2016). By applying a coupled land surface-subsurface model to simulate three-way interactions among river water, groundwater, and land surface processes at the same site used in our present study, Bisht et al. (2017) demonstrated that groundwater-river water interactions strongly modulate land-surface energy partitioning at the site by expanding the periodically inundated fraction of the riparian zone and enhancing moisture availability in the vadose zone via capillary rise in response to changes in river stage. Therefore, lateral river water-groundwater exchange could play an important role in determining how ecosystem fluxes will respond to changing hydroclimatic conditions in semiarid regions. However, the impacts of climate change on such ecosystems remains a significant knowledge gap.

Dryland ecosystems commonly demonstrate large interannual variability in net ecosystem exchange of CO_2 ($NEE = R_{eco} - GPP$, where R_{eco} is ecosystem respiration and GPP is gross primary production), and often alternate between acting as carbon sinks during wet years and as carbon sources during dry years (Biederman et al., 2017; Kwon et al., 2008; Scott et al., 2015). Drought conditions negatively impact ecosystem productivity, in large part due to plant physiological responses to both soil drought (low soil moisture content) and atmospheric drought (high vapor pressure deficit; Kwon et al., 2008). Dryland ecosystems generally rely on deep water stores to sustain ecosystem functioning during dry periods (Kwon et al., 2008; Miller et al., 2010; Prieto et al., 2014; Ryel et al., 2004). The distribution of soil moisture in semiarid ecosystems can be significantly influenced by the vegetation structure. For example, *Artemisia tridenata* (sagebrush) has been shown to influence the vertical distribution of moisture within the soil column through hydraulic redistribution, where the roots transport water from wetter soil layers to drier soil layers (Ryel et al., 2002, 2003). This redistribution of soil moisture can occur either upward or downward in the soil column and can affect the ability of the plant roots to reach deep groundwater. This phenomenon can have significant effects on ET, helping facilitate ecosystem transpiration under periods of high evaporative demand (Ryel et al., 2002). Use of deeper water stored by hydraulic redistribution can allow plants to photosynthesize when surface soils are dry, enhancing ecosystem productivity during periods of seasonal drought (Prieto et al., 2014; Ryel et al., 2004; Scott, Cable, & Hultine, 2008). Thus, ecosystem structure is an important driver of productivity in dryland ecosystems, since the rooting characteristics of the vegetation influence the extent to which plants can access deep soil moisture. The composition of the plant community influences the rate at which ecosystem carbon pools respond to changes in environmental drivers, with systems dominated by nonwoody species such as grasses responding more rapidly than ecosystems dominated by woody species such as shrubs (Scott et al., 2015).

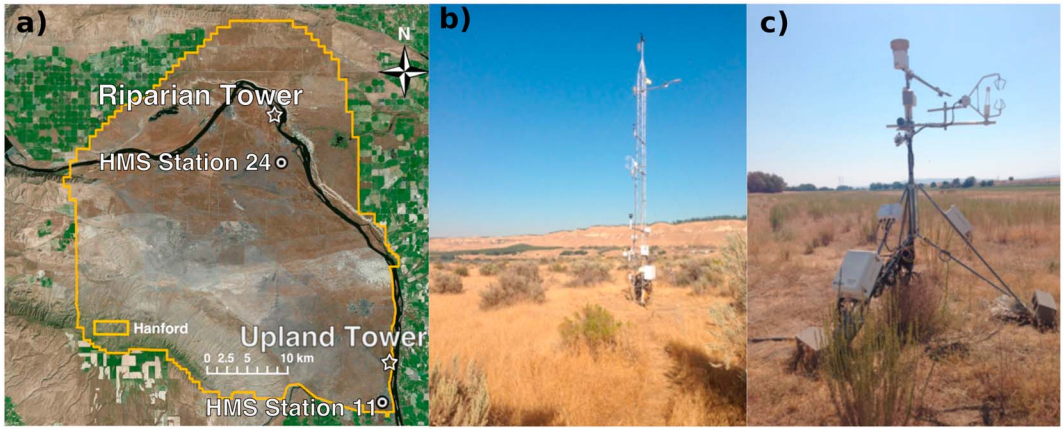

Figure 1. (a) Map of the Hanford Site in central Washington, USA, showing the locations of the eddy covariance towers and the Hanford Meteorological Stations (HMSs 11 and 24). (b) Photo of the upland site eddy covariance tower. (c) Photo of the riparian site eddy covariance tower.

In dryland ecosystems, moisture can be a significant driver of R_{eco} (Conant et al., 2004). There has been extensive research on the temperature sensitivity of ecosystem respiration, but in dryland ecosystems, moisture availability may play a more critical role (Liu et al., 2009). In wetter years, increases in GPP are often offset by greater R_{eco} (Scott et al., 2014, 2015). In some cases, increased precipitation can actually lead to decreased NEE magnitude when increases in R_{eco} exceed the increases in GPP (Scott et al., 2014). Additional research is needed to investigate how GPP and R_{eco} respond to changes in water availability and thus how this impacts the NEE of the ecosystem.

Despite the importance of dryland ecosystems to the global carbon, water, and energy budgets, land-surface fluxes remain relatively poorly studied in these ecosystems compared to mesic ecosystems. In this paper, we characterize the influence of water availability resulting from lateral groundwater-river water exchange on NEE, ET, and the surface energy balance at two distinct semiarid ecosystems located near the Columbia River in central Washington, USA. We collected 1 year of eddy covariance (EC) measurements from two flux sites: an upland sagebrush ecosystem fed mainly by rainfall and a riparian grassland ecosystem with groundwater access resulting from elevated river stage in the dry season. We examine how rooting-zone water availability is modulated by rainfall and lateral groundwater-river water exchange at the two sites, which consequently influences NEE, ET, and the partitioning of the surface energy balance. We attempt to address the following science questions: (1) How do rainfall and lateral groundwater-river water exchange influence ecosystem water availability and ET in semiarid ecosystems? (2) How might the partitioning of sensible and latent heat fluxes and seasonal patterns of NEE be modulated by water availability in response to rainfall and lateral groundwater-river water exchange at the sites?

2. Methods

2.1. Sites

This study was conducted at two sites located within the Hanford Area in central Washington, USA (Figure 1). The Hanford Site has a semiarid climate influenced by the Cascade mountain range to the west. The long-term average annual precipitation is 17 cm (Duncan et al., 2007). Most of the annual precipitation occurs during the late fall and winter, and snow accounts for 38% of the total precipitation from December through February (Duncan et al., 2007). We collected measurements at two distinct semiarid ecosystems within the Hanford Area located about 35 km apart with access to different levels of groundwater availability: an upland site (AmeriFlux site US-Hn1; 46.4089°N, 119.2750°W; Figure 1b) and a riparian site (AmeriFlux site US-Hn2; 46.6889°N, 119.4641°W; Figure 1c). The elevations of the upland and riparian sites are 118.6 and 117.6 m, respectively, based on the North American Vertical Datum of 1988. The upland site is a sagebrush ecosystem with a deep vadose zone at which the soil moisture input is fed by rainfall. Its vegetation consists of a mixture of shrubs and grasses. Shrub species include *Artemisia tridentata* (big sagebrush; 10% cover) and *Chrysothamnus viscidiflorus* (green rabbitbrush; <1% cover). Invasive weedy species include *Bromus tectorum* (cheatgrass; 70% cover) and *Salsola kali* (Russian thistle). Native grasses are

also present, including *Poa secunda* (sandberg bluegrass; <1% cover), *Pseudoroegneria spicata* (bluebunch wheatgrass; <1% cover), and *Stipa comate* (needle-and-thread grass; <1% cover). Based on previous measurements performed within the Hanford Area, the maximum rooting depths of the shrub species are 2.5 m or shallower (Sample et al., 2015). At this site, the soil texture in the top 30 cm is loamy sand (5% clay, 11% silt, and 84% sand), and the soil texture in the layer from 30 to 45 cm is sand (2% clay, 4% silt, and 94% sand). The riparian site is a grassland ecosystem at which plant available water is strongly modulated by lateral groundwater-river water exchange. Its vegetation consists primarily of invasive weedy species such as cheatgrass (40% cover), Russian thistle (5% cover), and *Centaurea repens* (diffuse knapweed; 5% cover). Native grasses are present, including *Sporobolus cryptandrus* (sand dropseed; <1% cover), *Poa bulbosa* (bulbous bluegrass; <1% cover), and *Agropyron dasystachyum* (thickspike wheatgrass; <1%). *Artemisia dracunculus* (tarragon), a native subshrub, is also present. Previous measurements in the Hanford area report maximum cheatgrass rooting depth between 50 and 160 cm (Sample et al., 2015). At this site, the soil texture in the top 45 cm is sand (2% clay, 8% silt, and 90% sand). For this study, we examined the measurements collected from January to December 2016 at both flux tower sites. Since measurements were not available for November–December 2015, we used the 2016 calendar year rather than the hydrologic year for our analysis.

2.2. EC Measurements

At each site, EC measurements of net ecosystem carbon dioxide and water vapor fluxes were made using an open-path infrared gas analyzer (Model LI-7500A, LI-COR, Lincoln, Nebraska, USA) and a 3-D sonic anemometer (Model CSAT3, Campbell Scientific, Logan, Utah, USA). At the upland site, the EC instruments were located at a height of 5 m. At the riparian site, the EC instruments were located at a height of 2.5 m. Raw 10-Hz data were stored on a data logger (CR5000, Campbell Scientific, Logan, Utah). Half-hourly fluxes were calculated from the raw data. The data were despiked (Vickers & Mahrt, 1997) and filtered for instrument malfunctions and out-of-range signals. Sonic anemometer data were rotated according to the double rotation method (Wilczak et al., 2001). Flux measurements were corrected for the effects of air density fluctuations caused by heat and water vapor transfer (Webb et al., 1980).

Gap filling, u_* filtering, and partitioning of the EC data sets were performed using the R package REddyProc (Wutzler et al., 2018). NEE was partitioned into gross primary productivity (GPP) and ecosystem respiration (R_{eco}) by fitting an exponential function of air temperature to the nighttime NEE data, as described by Reichstein et al. (2005).

Seasonal u_* thresholds were calculated on a seasonal basis according to the method described by Papale et al. (2006), and flux measurements below the thresholds were replaced with gap-filled values. The u_* thresholds ranged from 0.05 to 0.09 m/s (Table S1 in the supporting information). The marginal distribution sampling method was used to gap fill the flux measurements. Gap-filled data points were classified into three quality control (QC) categories in order to assess the reliability of the gap-filled data (QC 1, QC 2, and QC 3 in Tables S2 and S3), where QC 1 represents the most reliable values and QC 3 represents the least reliable values.

The percentage of missing flux data at both sites ranged from 15% to 29% in 2016, with the majority of gaps being less than 1 day. The majority of gap-filled data points corresponded to the highest-quality flag for gap-filled values (Tables S2 and S3). We estimated the error in NEE and ET associated with gap filling by using the gap filling procedure to fill artificially added gaps in the data set. For each site, we created two new data sets with added artificial gaps of the same duration as the original data gaps: one in which added gaps started the day after the original gaps ended and one in which the new gaps ended the day before the original gap started. We then compared the annual NEE and ET values for the data sets with artificial gaps added to the original data sets. Based on this approach, the error associated with data gaps was around ±10% for annual NEE and ±7% for annual ET.

2.3. Meteorological and River Stage Measurements

A variety of meteorological measurements were conducted at both flux tower sites, including air temperature, relative humidity, net radiation, soil temperature, soil volumetric water content, soil heat flux, and precipitation (Table 1). Meteorological data were collected and stored at 1-min frequency on a data logger (Models CR1000 and CR5000, Campbell Scientific, Logan, UT, USA). Hourly meteorological data from the stations nearest to each flux site were also obtained from the Hanford Meteorological Station (HMS)

Table 1
Heights of Tower Sensors and Depths of Soil Sensors Installed at the Upland and Riparian Sites

Sensor	Variables	Sensor heights or depths		Manufacturer
		Upland site	Riparian site	
LI-7500A	Carbon dioxide and water vapor concentrations	5 m	2.5 m	LI-COR, Lincoln, Nebraska
CSAT3	3-D wind components	5 m	2.5 m	Campbell Scientific, Logan, Utah
HMP45C	Air temperature and relative humidity	1, 2, 5, 8, and 10 m	2.5 m	Campbell Scientific, Logan, Utah
CNR2	Net shortwave and net longwave radiation	8 m (until 18 March 2016)	3 m	Kipp & Zonen, Delft, the Netherlands
CNR4	Net shortwave and net longwave radiation	8 m (after 18 March 2016)		Kipp & Zonen, Delft, the Netherlands
RM-Young 03002	Wind speed and direction	10 m		RM Young, Traverse City, Michigan
SI-111	Soil surface temperature	3.8 m		Apogee Instruments, Logan, Utah
109SS	Soil temperature	2.5, 5, 10, 15, and 20 cm	2.5, 5 cm	Campbell Scientific, Logan, Utah
CS616	Soil volumetric water content	2.5, 5, 10, 15, and 20 cm	5 cm	Campbell Scientific, Logan, Utah
HFP-01	Soil heat flux	5 and 20 cm	5 cm	Huskeflux Thermal Sensors, Delft, the Netherlands
HFPSC-01	Soil heat flux	5 and 20 cm		Huskeflux Thermal Sensors, Delft, the Netherlands
TE525	Precipitation	2 m	3 m	Texas Electronics, Texas

Monitoring Network (http://www.hanford.gov/page.cfm/HMS). HMS 11 is located ~5 km from the upland tower, and HMS 24 is located about 6 km from the riparian tower (Figure 1). In the case of rain gage failure at one of the tower sites, the precipitation data were filled using measurements from the nearest HMS. Thus, the hourly precipitation totals for this study period were gap free.

To evaluate the 2016 weather conditions in the context of the long-term climate of the area, we used long-term data from the PRISM Climate Group (http://prism.oregonstate.edu). We obtained the daily total precipitation and daily mean temperature for the period from 1986 to 2016 at 46.4089°N, 119.2750°W (the location of the upland tower). The 2016 PRISM precipitation data showed excellent agreement with the tower rain gage, with the annual total precipitation differing by less than 2 mm. We examined the annual and monthly anomalies in the 2016 precipitation and temperature relative to the 30 years prior to 2016 (1986–2015).

At the upland site, the river stage was monitored by a well located about 4.5 km downstream from the flux tower (Figure S1). At the riparian site, hourly river stage was measured at one upstream and one downstream location near the flux tower from 12 October 2016 to 2 August 2017 (Figure S1; INW LevelSCOUT Sensors, Kent, WA). Total pressure measured by the piezometers was converted to water elevation by subtracting the barometric pressure. An adjustment was also made to correct for the difference in elevation between the pressure transducer and the top of the piezometer, which was surveyed using real-time kinematic GPS. Since piezometer measurements were not available for the entire year of 2016, we developed statistical relationships between the available upstream and downstream piezometer measurements and hourly river discharge measurements from the Priest Rapids Dam to estimate the hourly river stage for the entire year. First, we built a generalized linear model (GLM; McCullagh & Nelder, 1989) using the GLM function in the statistical computing software R (R Core Team, 2015) for the available data set with 3,873 observations collected during the measured time period. The dependent variable was the river stage at the riparian site and the predictor variable was the measured river discharge obtained from U.S. Geological Survey's website (https://waterdata.usgs.gov/nwis/uv?site_no=12472800). The sample cross-correlation function (CCF) was applied to determine the time lags between river stage and discharge. Nearly equal maximum values of CCF occurred at −6, −5, and −4 hr with correlation values of 0.927, 0.966, and 0.960, respectively. The negative CCF values indicate that the time series of discharge leads the river stage. We implemented discharge and discharges lagged up to −10 hr as predictor variables in the GLM model

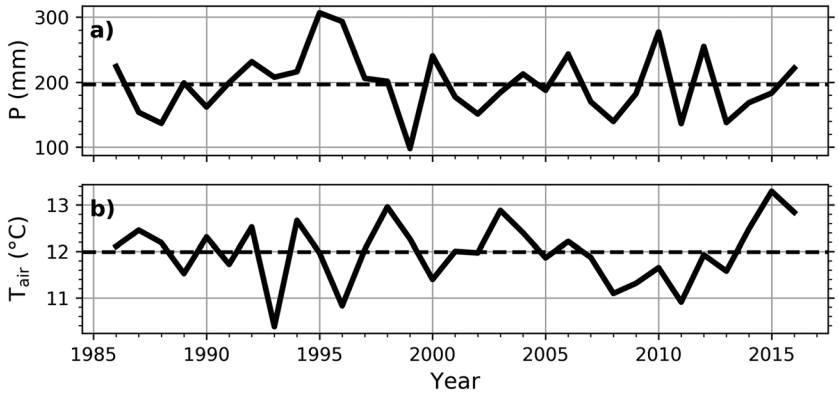

Figure 2. The annual total precipitation (a) and mean air temperature (b) at the upland tower location for the period from 1986 to 2016. The dashed lines represent the means for the 30-year period prior to 2016.

development. Second, we performed model selection based on Akaike information criterion (Akaike, 1974) in R's stepwise algorithm using both forward and backward searching directions. Discharge and −1-hr-lagged discharge were dropped as predictor variables during model selection. The lagged-regression models were used to predict water elevation at both the upstream and downstream locations near the riparian flux tower for the entire year of 2016. The goodness of fits were measured using R^2 values (1 − residual sum of squares/total sum of squares), which were 0.994 and 0.995 for the upstream and downstream locations, respectively. In addition, during 2016 several measurements of the water table depth were collected from a well located 418 m away from the riparian flux tower (Figure S1). From 16 August 2018 to 20 September 2018 piezometer measurements were also collected in the slough near the riparian site, 415 m away from the tower (Figure S1).

2.4. Water Balance Calculations

To estimate the groundwater uptake, we calculated the water budget closure at each site based on the precipitation and flux tower ET measurements. Using this approach, the deficit between the incoming and outgoing water in the system is used to infer the amount of groundwater uptake and stored soil water in the system.

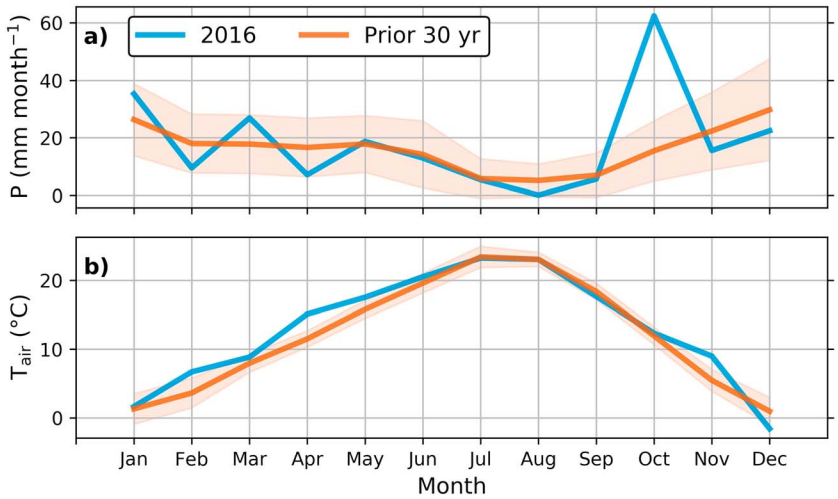

Figure 3. (a) The monthly total precipitation in 2016 (blue line) and the 30-year average monthly precipitation prior to 2016 (orange line, ±*SD*) at the upland tower location. (b) The monthly average air temperature in 2016 (blue line) and the 30-year average monthly air temperature prior to 2016 (orange line, ±*SD*).

Table 2
Monthly Average Values of Net Radiation (R_n, W/m^2), Air Temperature (T_{air}, °C), Soil Temperature (T_{soil}, °C), Relative Humidity (RH, fraction), Friction Velocity (u_*, m/s), Wind Speed (WS, m/s), and Volumetric Soil Water Content (SWC) at 5-cm Depth (m^3/m^3) at the Upland and Riparian Sites

	R_n (W/m^2)		T_{air} (°C)		T_{soil} (°C)		RH		u_* (m/s)		WS (m/s)		SWC (m^3/m^3)	
Month	Upland	Riparian	Upland	Riparian	Upland	Riparian	Upland	Riparian	Upland	Riparian	Upland	Riparian	Upland	Riparian
Jan	19.18	12.89	4.77	1.28	2.28	0.57	0.83	0.94	0.16	0.12	1.74	0.93	0.12	0.10
Feb	41.68	41.52	6.50	5.23	6.31	6.05	0.74	0.78	0.21	0.13	2.24	1.11	0.11	0.09
Mar	70.45	66.51	9.25	8.54	9.90	9.29	0.61	0.64	0.26	0.20	2.70	2.15	0.11	0.07
Apr	124.88	105.06	15.27	14.39	18.46	19.95	0.50	0.54	0.22	0.18	2.35	1.62	0.06	0.03
May	142.85	123.83	18.28	17.88	23.77	25.60	0.47	0.46	0.27	0.25	2.61	2.49	0.06	0.02
Jun	161.78	138.70	21.90	21.33	29.21	30.62	0.40	0.40	0.29	0.23	2.73	2.14	0.05	0.03
Jul	146.37	132.91	24.05	23.68	31.48	32.57	0.40	0.41	0.28	0.24	2.54	2.38	0.04	0.02
Aug	124.32	106.25	24.12	24.03	31.94	32.77	0.38	0.37	0.23	0.19	2.19	1.62	0.03	0.02
Sep	79.36	69.30	18.09	18.04	23.06	23.69	0.48	0.47	0.23	0.20	2.29	1.71	0.03	0.02
Oct	32.19	36.36	12.62	12.21	14.88	13.20	0.69	0.71	0.23	0.19	2.5q2	1.65	0.10	0.07
Nov	17.31	19.22	8.71	8.05	9.11	7.57	0.77	0.79	0.21	0.15	2.22	1.26	0.13	0.09
Dec	0.39	0.82	−1.64	−2.06	1.75	−1.49	0.80	0.77	0.20	0.16	2.17	1.47	0.12	0.05
Annual mean	83.62	75.42	14.00	12.8	16.87	18.07	0.67	0.58	0.24	0.19	2.40	1.69	0.08	0.05

Previous studies at the Hanford site suggest that the shallow subsurface material at the site is highly permeable with average hydraulic conductivity at about 3,100 m/day; thus, surface runoff seldom presents (Thorne et al., 2006; Williams et al., 2008). Therefore, the water budget can be represented as

$$G_w + P - ET = z\frac{\partial\theta}{\partial t}, \quad (1)$$

where G_w is the net groundwater uptake, P is precipitation, ET is evapotranspiration, z is the depth of the soil layer, θ is the volumetric soil water content in the entire soil layer, and $z\frac{\partial\theta}{\partial t}$ is the soil moisture storage. G_w represents the difference between groundwater uptake (U) by the ecosystem and leakage (L) from the soil layer ($G_w = U - L$). Given that only shallow soil moisture was measured at the flux sites, the total $z\frac{\partial\theta}{\partial t}$ cannot be accurately calculated. Thus, for our analysis we will examine the residual in the water balance, given by $\text{Res} = G_w - z\frac{\partial\theta}{\partial t}$, where the residual represents both net groundwater uptake and changes in the amount of stored soil moisture. The residual in this case is calculated as the difference between the ET and precipitation, as follows:

$$\text{Res} = ET - P. \quad (2)$$

Since ET was measured as half-hourly fluxes, a half-hourly time step was used for the calculations. The results are reported as aggregated monthly values.

3. Results

3.1. Meteorological and River Stage Conditions

Based on the long-term PRISM data set for the site, the annual precipitation in 2016 (222 mm) was greater than the mean annual precipitation of the 30-year base period (197 mm; Figure 2a). The 2016 mean air temperature (12.8 °C) was also greater than the 30-year mean (12.0 °C; Figure 2b). To investigate the seasonal anomalies in precipitation and temperature, we compared the monthly total precipitation and mean monthly air temperature in 2016 to the mean monthly values of the 30-year base period. In 2016, there was a large precipitation anomaly in October, which had much greater precipitation than the base period (Figure 3a). The high annual mean air temperature in 2016 was largely caused by warmer temperatures during the early growing season (February–June; Figure 3b). Monthly mean air temperatures for July–October 2016 were very similar to the base period.

Comparing the meteorological measurements at the two flux tower sites in 2016, the sites had fairly similar meteorological conditions. Net radiation was similar for the two sites, with the upland site having slightly greater net radiation than the riparian site (Table 2). Differences in average monthly net shortwave radiation between the two sites were less than 12 W/m^2. Soil temperature was usually slightly greater at the riparian site compared to the upland site (Table 2). The upland site generally had larger sensible heat fluxes than the riparian site (Figure 4). The relative humidity was fairly similar at the two sites (Table 2). The seasonal patterns of precipitation were very similar at the two sites, although the total annual precipitation was greater at the upland site than at the riparian site (224 vs.

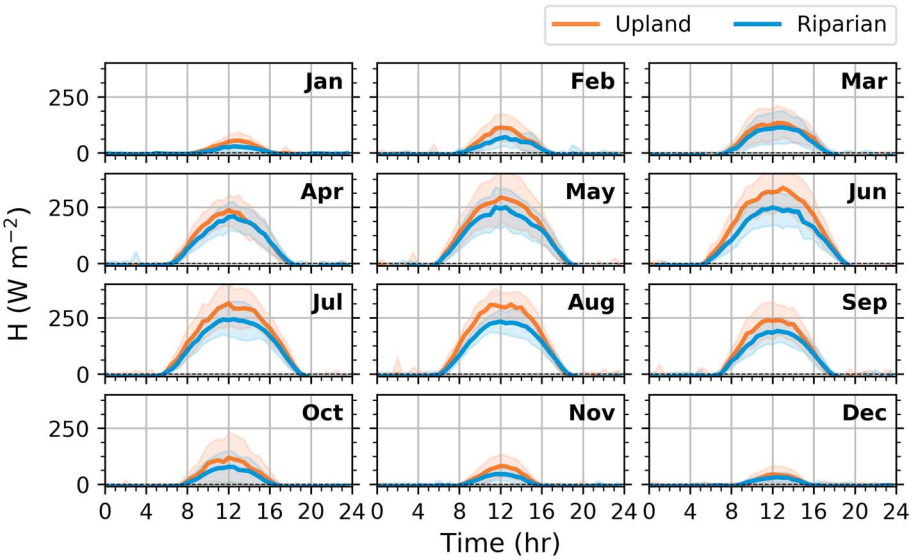

Figure 4. Comparison of the monthly diurnal average sensible heat flux (*H*) at the upland and riparian flux sites in 2016.

176 mm; Figure 5b and Table 3). The biggest difference in monthly precipitation between the two sites occurred in May, with the upland site receiving 16 mm more than the riparian site. This discrepancy between the two sites was likely attributed to the difference in local convective storms early in the summer. The seasonal patterns of shallow soil moisture were similar at the two sites (Figures 5 and 6 and Table 2), with the upland site having slightly greater soil water content than the riparian site. This is likely due to the differences in precipitation at the two sites, as well as differences in soil texture.

At the upland site, the mean river stage in 2016 was 105.34 m (standard deviation: 0.4265 m), which is 13.2 m below the tower elevation. The annual mean river stage at the riparian site, as represented by the average of the river stage at the upstream and downstream locations, was 114.51 m (standard deviation: 0.6424 m), which is 3.1 m below the tower elevation. Measurements collected at a well near the riparian site demonstrate that there was close agreement between the water table depth and the river stage (Figure 10). Additional piezometer measurements collected in the slough near the riparian site in August–September 2018 also demonstrate the similarity between the river stage and water table depth at the site (Figure S6).

3.2. Comparison of Water and Energy Balance Components at the Upland and Riparian Sites

Although the two sites had similar seasonal patterns of precipitation, they had very distinct seasonal patterns of ET. At the upland site, the monthly ET was largest in April and then declined through the growing season (Figures 7 and 8). In contrast, the riparian site maintained more consistent monthly ET values throughout the growing season, and the monthly total ET was the largest in July (Figure 7). At the riparian site, the residual in the water balance accounted for the majority of the ET during April–September (Figure 9). At both sites, during the spring and summer months the total ET exceeded the total precipitation and the residual in the water balance was positive (Figure 9). Both sites had negative residuals in January and October, when large precipitation pulses greatly exceeded the monthly ET (Figure S5). At both sites, the residual accounted for a large fraction of the total ET during the spring and summer months (Figure 9). The ratio of the residual to the total ET (Res/ET) was greater at the riparian site than at the upland site during April–July. In August, there was no precipitation at either site, resulting in a Res/ET ratio of 1. During the summer months (June–August), the ET at the riparian site was 1.3 to 2.7 times greater than that at the upland site. On an annual basis, the total ET was slightly higher at the riparian site than at the upland site (277 vs. 250 mm, Table 3). At the riparian site, the total annual ET was 1.57 times the total annual precipitation. In contrast, at the upland site the total annual ET was comparable to the total annual precipitation (250 and 224 mm, respectively).

The distinct patterns of ET (and latent heat flux) at the two sites corresponded to a large difference in the energy balance partitioning between the two sites. The upland site had a larger annual Bowen ratio than

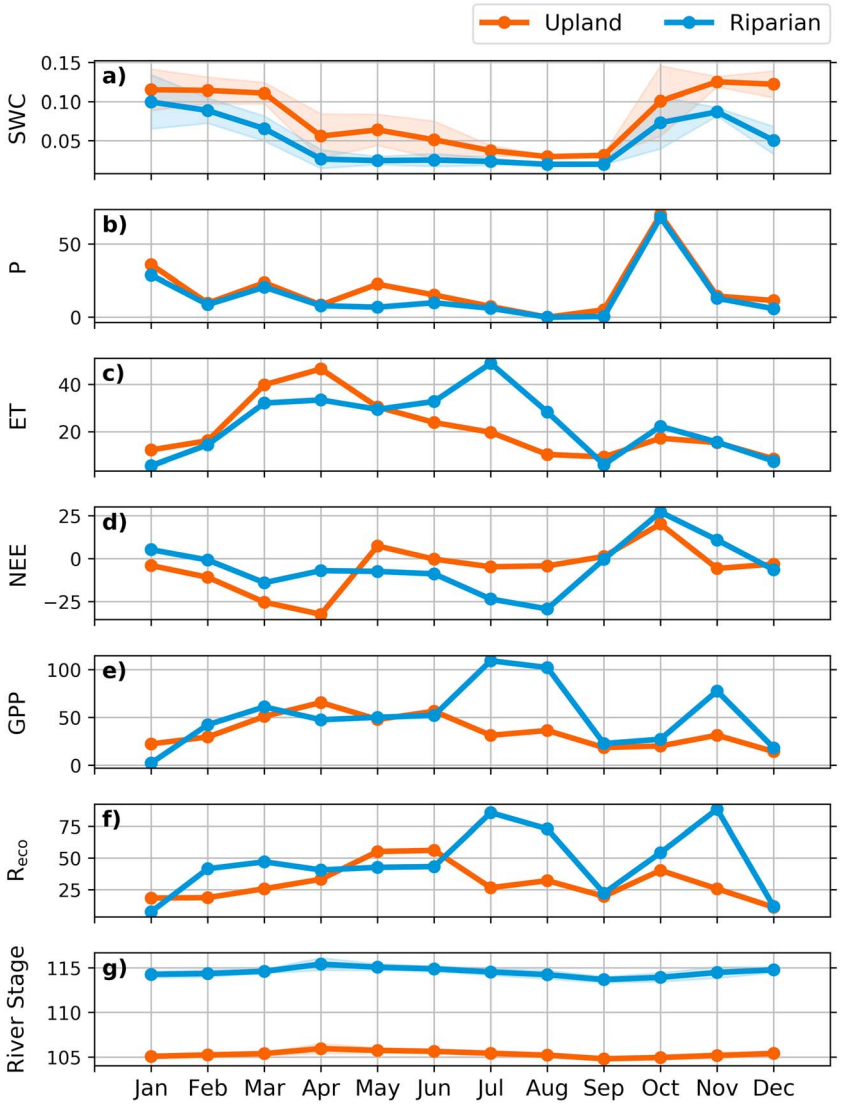

Figure 5. Data collected at the upland and riparian sites in 2016. (a) Monthly average (±*SD*) volumetric soil water content (SWC) at 5-cm depth. (b–f) Monthly total precipitation (*P*, mm/month), evapotranspiration (*ET*, mm/month), net ecosystem carbon flux (*NEE*, gC·m^{-2}·month^{-1}), gross primary productivity (*GPP*, gC·m^{-2}·month^{-1}), and ecosystem respiration (R_{eco}, gC·m^{-2}·month^{-1}). (g) Monthly average (±*SD*) river stage (m) near the riparian site.

the riparian site (2.4 vs. 1.7). The largest differences in the Bowen ratios between the two sites occurred during the summer months. During these months (June–August), the riparian site had higher latent heat fluxes (Figure 8) and lower sensible heat fluxes (Figure 4) during the daytime compared to those at the upland site. Thus, the riparian site had a lower Bowen ratio than the upland site during the summer months (Table 3), with the largest difference between the two sites occurring in August (9.9 vs. 2.7).

3.3. Comparison of CO_2 Fluxes at the Upland and Riparian Sites

The proximity and similar meteorological conditions of the two flux tower sites allow us to examine the effects of groundwater availability and vegetation structure on the ecosystem fluxes. Despite having similar meteorological conditions, the two sites demonstrated very different seasonal patterns in the ecosystem CO_2 fluxes. The two flux tower sites had distinct seasonal patterns of NEE. At the upland site, the magnitude of NEE was maximized in April (−32 gC·m^{-2}·month^{-1}, with $NEE < 0$ indicating net carbon uptake) and then declined as the growing season progressed (Figures 5 and 11 and Table 3). In contrast, NEE at the riparian site was fairly consistent during the spring and early summer, and its magnitude was maximized during

Table 3
Monthly and Annual Integrated Precipitation (P, mm), Evapotranspiration (ET, mm), NEE (gC/m^2), Gross Primary Production (GPP, gC/m^2), and Ecosystem Respiration (R_{eco}, gC/m^2), Monthly and Annual Average Sensible Heat Flux (H, W/m^2) and Latent Heat Flux (LE, W/m^2), and Monthly and Annual Bowen Ratios at the Upland and Riparian Sites

	P (mm)		*ET* (mm)		*NEE* (gC/m^2)		*GPP* (gC/m^2)		R_{eco} (gC/m^2)		*H* (W/m^2)		*LE* (W/m^2)		Bowen ratio	
Month	Upland	Riparian	Upland	Riparian	Upland	Riparian	Upland	Riparian	Upland	Riparian	Upland	Riparian	Upland	Riparian	Upland	Riparian
Jan	35.81	28.70	12.28	5.62	−3.99	5.23	22.28	2.19	18.29	7.42	5.03	1.95	11.39	5.22	0.44	0.37
Feb	9.65	8.64	16.18	14.44	−10.84	−0.79	29.50	42.35	18.66	41.56	13.54	9.22	16.00	14.28	0.85	0.65
Mar	23.62	20.57	39.89	32.13	−25.30	−13.97	51.03	61.01	25.74	47.04	24.95	21.52	36.79	29.64	0.68	0.73
Apr	8.38	7.87	46.59	33.44	−32.37	−6.97	65.58	47.53	33.22	40.57	58.66	53.06	44.12	31.68	1.33	1.67
May	22.61	6.86	30.47	29.47	7.36	−7.43	47.84	50.09	55.20	42.66	86.16	71.90	27.88	26.96	3.09	2.67
Jun	15.24	9.91	23.89	32.80	−0.28	−8.83	56.42	52.08	56.14	43.25	108.63	78.45	22.52	30.91	4.82	2.54
Jul	7.37	6.10	19.73	48.97	−4.72	−23.47	31.23	109.27	26.51	85.81	97.05	77.02	17.96	44.55	5.40	1.73
Aug	0.00	0.00	10.33	28.33	−4.17	−29.21	36.30	102.20	32.13	72.99	92.90	68.59	9.37	25.76	9.91	2.66
Sep	5.08	0.51	9.31	6.11	1.28	−0.40	18.42	22.61	19.71	22.21	58.37	46.34	8.80	5.76	6.63	8.04
Oct	70.10	68.20	17.22	22.25	20.15	27.10	20.11	27.14	40.25	54.24	16.57	9.83	15.87	20.49	1.04	0.48
Nov	14.48	12.95	15.36	15.57	−5.68	10.86	31.34	77.66	25.66	88.52	5.11	1.70	14.65	14.85	0.35	0.11
Dec	11.43	5.84	8.48	7.54	−3.16	−6.47	14.20	18.08	11.04	11.61	−2.08	−0.42	7.91	7.03	−0.26	−0.06
Annual	223.77	176.15	249.72	276.66	−61.72	−54.35	424.26	612.23	362.55	557.87	47.07	36.60	19.44	21.43	2.42	1.71

August ($-29\ gC{\cdot}m^{-2}{\cdot}month^{-1}$; Figure 5 and Table 3). NEE was more negative at the upland site than at the riparian site from January–April; however, from May to August, NEE was more negative at the riparian site than at the upland site.

The partitioning results indicate that the distinct seasonal patterns in NEE at the two sites were driven primarily by differences in GPP during the growing season. At the upland site, GPP was maximized in April, while at the riparian site GPP was the largest during July and August (Figure 5 and Table 3). At the end of the growing season, the magnitude of the cumulative NEE was larger at the riparian site than at the upland site (Figure 6). The magnitude of the cumulative NEE experienced substantial reductions at both sites with the onset of the fall precipitation, but the largest change occurred at the riparian site (Figure 6). In November, the riparian site was a carbon source, while the upland site was a carbon sink (Figure 5 and Table 3). Although the riparian site had greater GPP than the upland site in November, it also had much greater R_{eco} (Figure 5 and Table 3). The total annual GPP was greater at the riparian site than at the upland site (612 vs. 424 gC/m^2; Table 3). However, the annual total ecosystem respiration was also greater at the riparian site than at the upland site (558 vs. 363 gC/m^2; Table 3). Thus, the magnitude of the annual NEE in 2016 was larger at the upland site than at the riparian site (−62 vs. −54 gC/m^2).

4. Discussion

4.1. Impacts of Lateral Groundwater-River Water Exchange on Ecosystem Water Availability

Our results indicate that the riparian site was dependent on groundwater uptake from sources in addition to rainfall for a large portion of its water balance, while the upland site was not. The differences between the total precipitation and the total ET on an annual basis can provide information about the amount of water uptake at each site. It should be noted that although surface runoff could occur when precipitation is very high (e.g., during the large precipitation event in October; Figure 6), such events were rare and should not have a large impact on the annual water balance components. Moreover, such events did not occur during the growing season, which was characterized by small and intermediate rainfall events. Since the change in soil water storage should not be large on an annual basis, the difference between the total annual ET and precipitation indicates the extent to which the ecosystem depends on groundwater uptake for its water usage. The similar values for total annual ET and precipitation at the upland site (250 vs. 224 mm) suggest that there was not a significant amount of groundwater uptake. In contrast, the large difference between the total annual ET and precipitation at the riparian site (277 vs. 176 mm) suggests that groundwater uptake accounted for a large portion of the ET.

The strong relationship between water table depth and river stage (Figure 10) suggests that plant available water to support ET at the riparian site is directly driven by the lateral exchange of river water and groundwater. That is, during the dry season (i.e., May to August) when rainfall is nearly absent, river water intrudes into the subsurface in response to elevated river stage, which increases the groundwater table and hence soil moisture to support ET. The phenomenon of groundwater

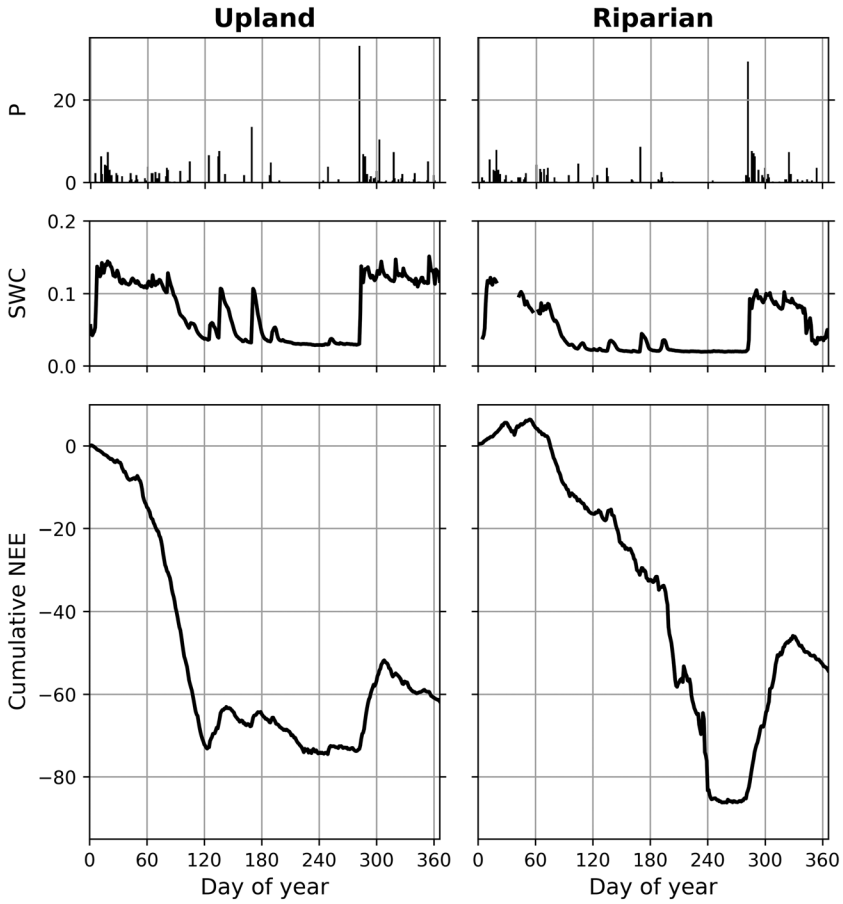

Figure 6. Daily precipitation (*P*, mm), volumetric soil water content (SWC), and cumulative net ecosystem carbon flux (*NEE*, gC/m^2) at the upland and riparian flux sites in 2016.

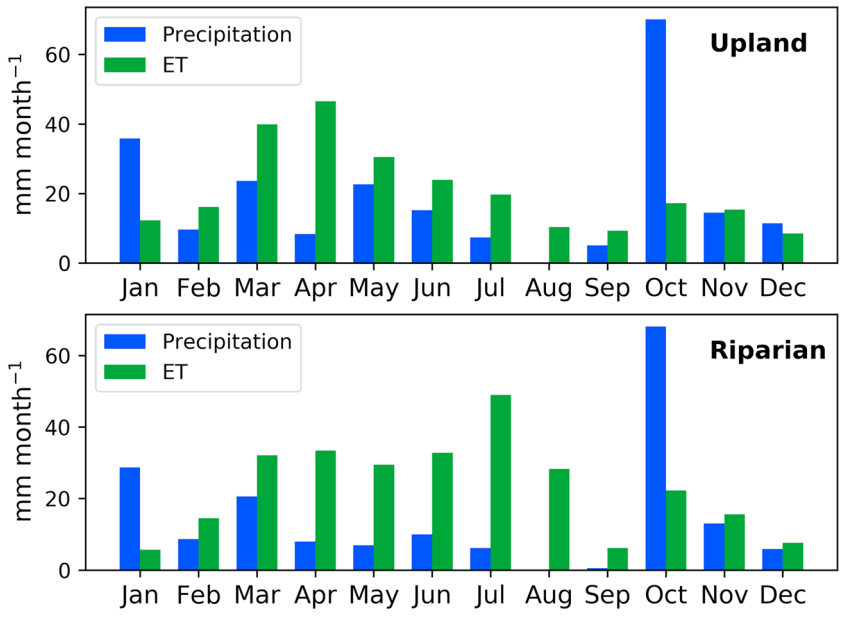

Figure 7. Comparison of the total precipitation (*P*, mm/month) and evapotranspiration (*ET*, mm/month) at the upland and riparian flux sites in 2016.

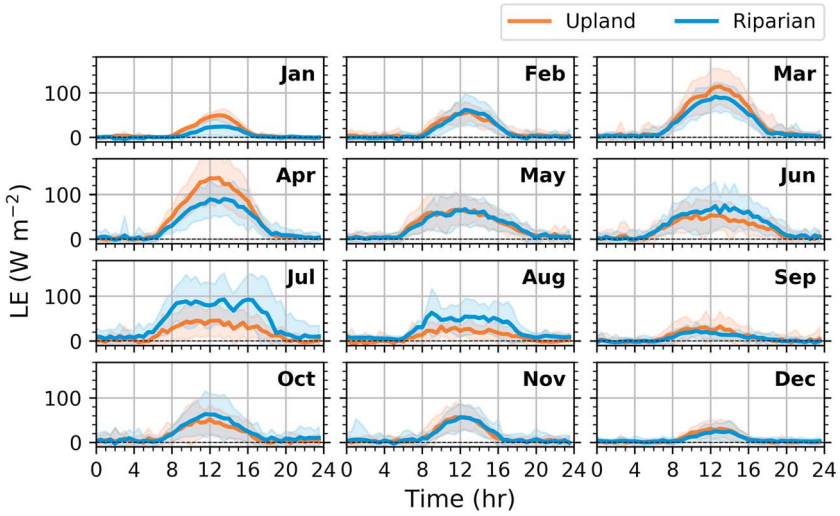

Figure 8. Comparison of the monthly diurnal average latent heat flux (LE) at the upland and riparian flux sites in 2016.

uptake enhancing ET during the dry season in sites with a shallow water table was also observed in a previous study that compared a semiarid riparian shrubland, woodland, and grassland to a nearby upland grassland ecosystem (Scott et al., 2014). At our site, the close agreement between the river stage and water table depth measurements indicates that the river stage is a good proxy for the water table depth. During 2016, the river stage at the riparian site ranged from 1.1 to 4.4 m below the tower elevation. Previous studies in sites with shallow water tables have demonstrated that the capillary rise of groundwater can recharge soil moisture in shallower layers above the water table, allowing vegetation to access groundwater resources even when the water table is deeper than the vegetation rooting depth (Chimner & Cooper, 2004; Thorburn & Walker, 1993).

The monthly water balance components demonstrate that groundwater uptake was a critical driver of the seasonal patterns of ET. At the upland site, where groundwater uptake was not observed, the residual in the water balance indicates the amount of water storage in the soil. At this site, there were large negative residuals in January and October corresponding to the large precipitation pulses, indicating soil water storage. From February through September, the positive residuals indicate the portion of the ET from stored soil moisture. The total ET decreased at the upland site every month from April through September, suggesting that ET became increasingly constrained by water availability as the stored soil water was depleted. In contrast, the riparian site maintained high ET during the spring and summer, with the greatest monthly ET occurring in July. During the summer months, the residual accounted for the majority of the total ET at the riparian site (70–100%, Figure 9). Since it is unlikely that the stored soil moisture was drastically different between the two sites, and the annual total ET greatly exceeded the annual precipitation at the riparian site, this indicates that groundwater uptake played a critical role in supporting ET during the spring and summer months.

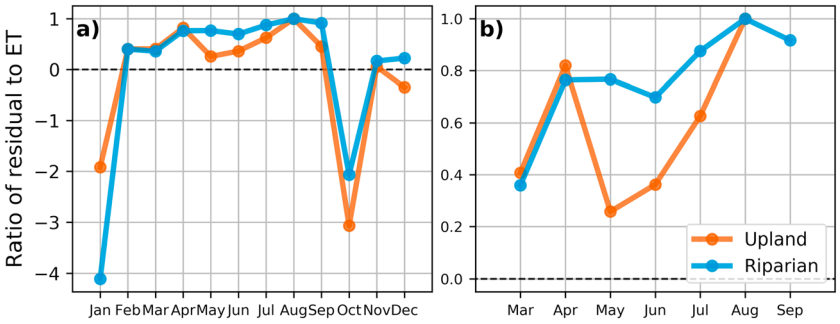

Figure 9. Ratio of the residual in the water balance (Res) to the total evapotranspiration (ET). (a) The monthly values of Res/ET for each month in 2016. (b) The values for March–September in greater detail.

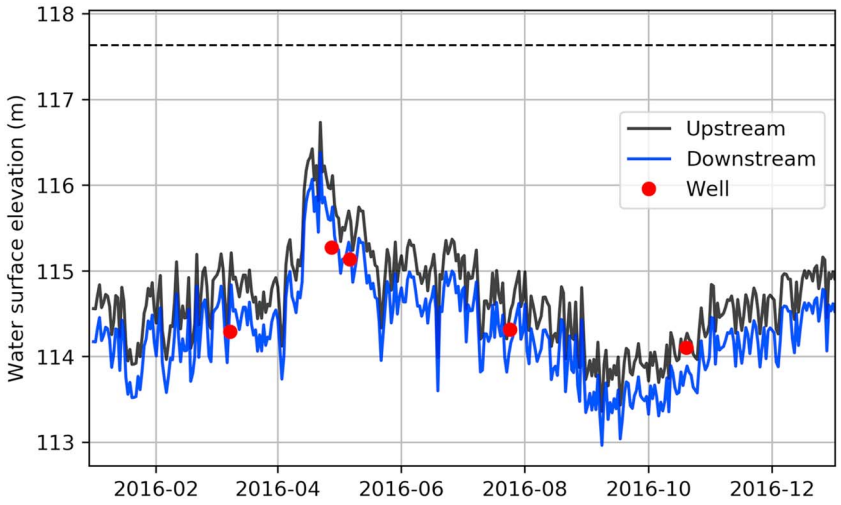

Figure 10. Daily average river stage (m) measured at the upstream and downstream piezometer locations near the riparian flux tower and water table elevation (m) measured at a nearby well. The dashed line indicates the elevation of the ground surface at the riparian flux tower location.

Although the two sites had very different seasonal patterns of ET, the seasonal patterns of shallow soil water content were very similar for the two sites (Figure 5a). This result indicates that the shallow volumetric soil water content was a poor indicator of ecosystem water availability and did not capture changes in water availability due to groundwater uptake or changes in moisture storage in deeper soil layers.

4.2. Water Availability Modulates Ecosystem ET and NEE

Our results demonstrate that lateral groundwater-river water exchange had a substantial impact on the partitioning of the surface energy budget at the riparian site, particularly during the summer months. During the summer months, at the riparian site the increased water availability from groundwater uptake enhanced the latent heat flux and reduced the Bowen ratio relative to the upland site. These results are consistent with previous modeling studies demonstrating the impact of shallow water tables on the latent heat flux and energy balance partitioning (Bisht et al., 2017; Maxwell & Condon, 2016).

The relationship between NEE and ET suggests that water availability was a critical driver of NEE in these ecosystems. The distinct seasonal patterns of NEE at the upland and riparian sites corresponded well to the

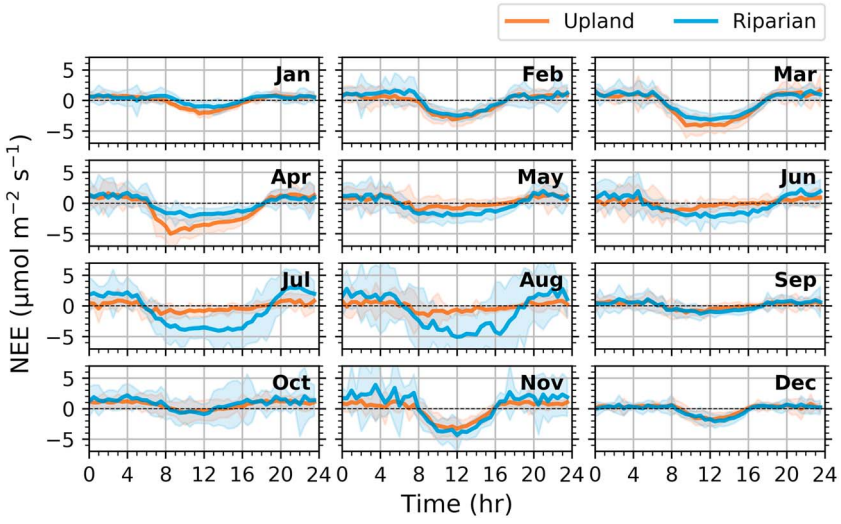

Figure 11. Comparison of the monthly diurnal average net ecosystem exchange of CO_2 (NEE) at the upland and riparian flux sites in 2016.

seasonal patterns of ET (Figure 11). The upland site had greater NEE magnitude and ET during the spring but lower NEE magnitude and ET during the summer months. In contrast, the riparian site maintained greater values of both NEE magnitude and ET during the drier summer months. Our results suggest that NEE at the upland site was restricted during the drier summer months due to lack of available water, as indicated by the reduced ET during these months. In contrast, the riparian site was able to maintain higher GPP during the dry months due to greater water availability than the upland site, as indicated by the greater values of ET. The pattern of enhanced ET and carbon uptake at the riparian site compared to the upland site is similar to that observed in Scott et al. (2014).

In determining the factors driving the enhanced ET at the riparian site during the dry months, it is important to consider differences in both meteorological conditions and vegetation structure. The upland site received more annual total precipitation than the riparian site (224 vs. 176 mm), indicating that the enhanced ET at the riparian site was not caused by differences in precipitation. In addition, the differences in vegetation type were unable to explain the enhanced ET at the riparian site relative to the upland site during the summer months. Previous studies have demonstrated that the rooting characteristics of shrub species such as sagebrush help enhance plant available soil moisture and facilitate higher transpiration and productivity during periods of water limitation (Prieto et al., 2014; Ryel et al., 2002, 2004). Thus, in the absence of groundwater availability, we would expect the upland site to be more resistant to water limitations than the riparian site, since the shrub species at this site have deeper roots to access stored soil moisture during periods of water stress.

Our results demonstrate that the response of R_{eco} to available moisture is a critical driver of annual NEE and that increases in GPP in response to increased water availability can be offset by enhanced R_{eco}. This result is consistent with previous studies demonstrating the sensitivity of ecosystem respiration in dryland ecosystems to precipitation events and changes in moisture availability (Conant et al., 2004; Jenerette et al., 2009; Liu et al., 2009; Scott et al., 2014). Both the upland and riparian sites experienced substantial respiration pulses with the onset of fall precipitation. Although the riparian site had larger cumulative NEE at the end of the growing season than the upland site, this was offset by larger R_{eco} in response to fall precipitation.

5. Conclusions

In this study, we have investigated the relationship between ecosystem available water and land-surface water, energy, and carbon fluxes using 1 year of EC data from two semiarid ecosystems. Our results demonstrate that groundwater access resulting from lateral groundwater-river water exchange can be a critical driver of NEE and ET in semiarid ecosystems. Due to the lack of water sources apart from rainfall, NEE at the upland site was strongly constrained by moisture availability during the summer months. In contrast, groundwater uptake resulting from river water intrusion into the subsurface allowed the riparian site to maintain high NEE magnitude and ET during the dry months, when NEE would be restricted by water availability in the absence of groundwater access. In areas where groundwater is available as a result of groundwater-river water exchange or convergence of groundwater driven by topography, it can account for a large portion of the water budget during the growing season and can dramatically alter the surface energy balance and the seasonal patterns of NEE and ET.

Improving our understanding of the role of groundwater in ecosystem carbon cycling is crucial to understanding how semiarid ecosystems will respond to future changes in climate. Water availability in many ecosystems is driven not only by precipitation but also by groundwater availability in response to large-scale hydroclimatic conditions. Thus, groundwater availability can fundamentally alter how an ecosystem will respond to changes in climate conditions. Longer-term measurements of the interannual variability in these ecosystems are needed to further examine the relationships between the ecosystem fluxes and the groundwater and climate conditions.

Acknowledgments
We thank many participants for their assistance in the field. We thank Kenton Rod for providing information about the soil texture at both sites. We are grateful to two anonymous reviewers for their constructive comments that improved the manuscript. We acknowledge support from the U.S. Department of Energy (DOE) Office of Biological and Environmental Research (BER) as part of BER's Subsurface Biogeochemical Research Program (SBR) at the Pacific Northwest National Laboratory (PNNL). PNNL is operated by Battelle Memorial Institute for the U.S. DOE under contract DE-AC05-76RLO1830. According to the AGU Publications Data Policy, the data used in this study are deposited in a public domain repository (https://doi.org/10.6084/m9.figshare.6406568.v2). Long-term climate data used in this study were obtained from PRISM Climate Group, Oregon State University, http://prism.oregonstate.edu, created 5 October 2017.

References

Ahlström, A., Raupach, M. R., Schurgers, G., Smith, B., Arneth, A., Jung, M., et al. (2015). The dominant role of semi-arid ecosystems in the trend and variability of the land CO_2 sink. *Science*, *348*(6237), 895–899. https://doi.org/10.1126/science.aaa1668

Akaike, H. (1974). A new look at the statistical model identification. *IEEE Transactions on Automatic Control*, *19*(6), 716–723. https://doi.org/10.1109/TAC.1974.1100705

Biederman, J. A., Scott, R. L., Bell, T. W., Bowling, D. R., Dore, S., Garatuza-Payan, J., et al. (2017). CO_2 exchange and evapotranspiration across dryland ecosystems of southwestern North America. *Global Change Biology*. Retrieved from https://doi.org/10.1111/gcb.13686/full

Bisht, G., Huang, M., Zhou, T., Chen, X., Dai, H., Hammond, G. E., et al. (2017). Coupling a three-dimensional subsurface flow and transport model with a land surface model to simulate stream–aquifer–land interactions (CP v1.0). *Geoscientific Model Development*, *10*(12), 4539–4562. https://doi.org/10.5194/gmd-10-4539-2017

Chimner, R. A., & Cooper, D. J. (2004). Using stable oxygen isotopes to quantify the water source used for transpiration by native shrubs in the San Luis Valley, Colorado U.S.A. *Plant and Soil*, *260*(1/2), 225–236. https://doi.org/10.1023/B:PLSO.0000030190.70085.e9

Conant, R. T., Dalla-Betta, P., Klopatek, C. C., & Klopatek, J. M. (2004). Controls on soil respiration in semiarid soils. *Soil Biology and Biochemistry*, *36*(6), 945–951. https://doi.org/10.1016/j.soilbio.2004.02.013

R Core Team (2015). R: A language and environment for statistical computing [Internet]. Vienna, Austria: R Foundation for Statistical Computing; 2014.

Dai, A. (2012). Increasing drought under global warming in observations and models. *Nature Climate Change*, *3*(1), 52–58. https://doi.org/10.1038/nclimate1633

Duncan, J. P., Burk, K. W., Chamness, M. A., Fowler, R. A., Fritz, B. G., Hendrickson, P. L., et al. (2007). Hanford Site National Environmental Policy Act (NEPA) Characterization, Rep. PNNL-6415 Rev. 18 (No. PNNL-6415 Rev 18). Pacific Northwest National Laboratory, Richland, WA, USA. https://doi.org/10.2172/919702

Green, T. R., Taniguchi, M., Kooi, H., Gurdak, J. J., Allen, D. M., Hiscock, K. M., et al. (2011). Beneath the surface of global change: Impacts of climate change on groundwater. *Journal of Hydrology*, *405*(3–4), 532–560. https://doi.org/10.1016/j.jhydrol.2011.05.002

Huang, J., Yu, H., Guan, X., Wang, G., & Guo, R. (2015). Accelerated dryland expansion under climate change. *Nature Climate Change*, *6*(2), 166–171 https://doi.org/10.1038/nclimate2837

Huang, L., He, B., Chen, A., Wang, H., Liu, J., Lű, A., & Chen, Z. (2016). Drought dominates the interannual variability in global terrestrial net primary production by controlling semi-arid ecosystems. *Scientific Reports*, *6*(1), 24639. https://doi.org/10.1038/srep24639

Jenerette, G. D., Scott, R. L., Barron-Gafford, G. A., & Huxman, T. E. (2009). Gross primary production variability associated with meteorology, physiology, leaf area, and water supply in contrasting woodland and grassland semiarid riparian ecosystems. *Journal of Geophysical Research*, *114*, G04010. https://doi.org/10.1029/2009JG001074

Kløve, B., Ala-Aho, P., Bertrand, G., Gurdak, J. J., Kupfersberger, H., Kværner, J., et al. (2014). Climate change impacts on groundwater and dependent ecosystems. *Journal of Hydrology*, *518*, 250–266. https://doi.org/10.1016/j.jhydrol.2013.06.037

Kwon, H., Pendall, E., Ewers, B. E., Cleary, M., & Naithani, K. (2008). Spring drought regulates summer net ecosystem CO_2 exchange in a sagebrush-steppe ecosystem. *Agricultural and Forest Meteorology*, *148*(3), 381–391. https://doi.org/10.1016/j.agrformet.2007.09.010

Leng, G., Huang, M., Voisin, N., Zhang, X., Asrar, G. R., & Leung, L. R. (2016). Emergence of new hydrologic regimes of surface water resources in the conterminous United States under future warming. *Environmental Research Letters*, *11*(11). https://doi.org/10.1088/1748-9326/11/11/114003

Liu, W., Zhang, Z., & Wan, S. (2009). Predominant role of water in regulating soil and microbial respiration and their responses to climate change in a semiarid grassland. *Global Change Biology*, *15*(1), 184–195. https://doi.org/10.1111/j.1365-2486.2008.01728.x

Maxwell, R. M., & Condon, L. E. (2016). Connections between groundwater flow and transpiration partitioning. *Science*, *353*(6297), 377–380. https://doi.org/10.1126/science.aaf7891

McCullagh, P., & Nelder, J. A. (1989). *Generalized linear models* (2nd ed.). Washington, DC: CRC Press. https://doi.org/10.1007/978-1-4899-3242-6

Miller, G. R., Chen, X., Rubin, Y., Ma, S., & Baldocchi, D. D. (2010). Groundwater uptake by woody vegetation in a semiarid oak savanna. *Water Resources Research*, *46*, W10503. https://doi.org/10.1029/2009WR008902

Mote, P. W., & Salathé, E. P. (2010). Future climate in the Pacific northwest. *Climatic Change*, *102*(1–2), 29–50. https://doi.org/10.1007/s10584-010-9848-z

Papale, D., Reichstein, M., Aubinet, M., Canfora, E., Bernhofer, C., Kutsch, W., et al. (2006). Towards a standardized processing of net ecosystem exchange measured with eddy covariance technique: Algorithms and uncertainty estimation. *Biogeosciences*, *3*(4), 571–583. https://doi.org/10.5194/bg-3-571-2006

Poulter, B., Frank, D., Ciais, P., Myneni, R. B., Andela, N., Bi, J., et al. (2014). Contribution of semi-arid ecosystems to interannual variability of the global carbon cycle. *Nature*, *509*(7502), 600–603. https://doi.org/10.1038/nature13376

Prieto, I., Pugnaire, F. I., & Ryel, R. J. (2014). Water uptake and redistribution during drought in a semiarid shrub species. *Functional Plant Biology*, *41*(8), 812–819. https://doi.org/10.1071/FP13300

Reichstein, M., Falge, E., Baldocchi, D., Papale, D., Aubinet, M., Berbigier, P., et al. (2005). On the separation of net ecosystem exchange into assimilation and ecosystem respiration: Review and improved algorithm. *Global Change Biology*, *11*(9), 1424–1439. https://doi.org/10.1111/j.1365-2486.2005.001002.x

Rupp, D. E., Abatzoglou, J. T., & Mote, P. W. (2017). Projections of 21st century climate of the Columbia River Basin. *Climate Dynamics*, *49*(5–6), 1783–1799. https://doi.org/10.1007/s00382-016-3418-7

Ryel, R. J., Caldwell, M. M., Leffler, A. J., & Yoder, C. K. (2003). Rapid soil moisture recharge to depth by roots in a stand of Artemisia tridentata. *Ecology*, *84*(3), 757–764. https://doi.org/10.1890/0012-9658(2003)084[0757:RSMRTD]2.0.CO;2

Ryel, R. J., Caldwell, M. M., Yoder, C. K., Or, D., & Leffler, A. J. (2002). Hydraulic redistribution in a stand of Artemisia tridentata: Evaluation of benefits to transpiration assessed with a simulation model. *Oecologia*, *130*(2), 173–184. https://doi.org/10.1007/s004420100794

Ryel, R. J., Leffler, A. J., Peek, M. S., Ivans, C. Y., & Caldwell, M. M. (2004). Water conservation in Artemisia tridentata through redistribution of precipitation. *Oecologia*, *141*(2), 335–345. https://doi.org/10.1007/s00442-003-1421-2

Sample, B. E., Lowe, J., Seeley, P., Markin, M., McCarthy, C., Hansen, J., & Aly, A. H. (2015). Depth of the biologically active zone in upland habitats at the Hanford Site, Washington: Implications for remediation and ecological risk management: Biointrusion at the Hanford Site, Washington. *Integrated Environmental Assessment and Management*, *11*(1), 150–160. https://doi.org/10.1002/ieam.1581

Scott, R. L., Biederman, J. A., Hamerlynck, E. P., & Barron-Gafford, G. A. (2015). The carbon balance pivot point of southwestern U.S. semiarid ecosystems: Insights from the 21st century drought. *Journal of Geophysical Research: Biogeosciences*, *120*, 2612–2624. https://doi.org/10.1002/2015JG003181

Scott, R. L., Cable, W. L., & Hultine, K. R. (2008). The ecohydrologic significance of hydraulic redistribution in a semiarid savanna. *Water Resources Research*, *44*, W02440. https://doi.org/10.1029/2007WR006149

Scott, R. L., Cable, W. L., Huxman, T. E., Nagler, P. L., Hernandez, M., & Goodrich, D. C. (2008). Multiyear riparian evapotranspiration and groundwater use for a semiarid watershed. *Journal of Arid Environments*, *72*(7), 1232–1246. https://doi.org/10.1016/j.jaridenv.2008.01.001

Scott, R. L., Huxman, T. E., Barron-Gafford, G. A., Darrel Jenerette, G., Young, J. M., & Hamerlynck, E. P. (2014). When vegetation change alters ecosystem water availability. *Global Change Biology*, *20*(7), 2198–2210. https://doi.org/10.1111/gcb.12511

Scott, R. L., James Shuttleworth, W., Goodrich, D. C., & Maddock, T. III (2000). The water use of two dominant vegetation communities in a semiarid riparian ecosystem. *Agricultural and Forest Meteorology*, *105*(1–3), 241–256. https://doi.org/10.1016/S0168-1923(00)00181-7

Taylor, R. G., Scanlon, B., Döll, P., Rodell, M., van Beek, R., Wada, Y., et al. (2013). Ground water and climate change. *Nature Climate Change*, *3*(4), 322–329. https://doi.org/10.1038/nclimate1744

Thorburn, P. J., & Walker, G. R. (1993). The source of water transpired by *Eucalyptus camaldulensis*: Soil, groundwater, or streams? In J. R. Ehleringer, A. E. Hall, & G. D. Farquhar (Eds.), *Stable isotopes and plant carbon-water relations* (pp. 511–527). San Diego: Academic Press. https://doi.org/10.1016/B978-0-08-091801-3.50042-8

Thorne, P. D., Bergeron, M. P., Williams, M. D., & Freedman, V. L. (2006). Groundwater data package for Hanford assessments, Rep. PNNL-14753 (No. PNNL-14753 Rev. 1). Richland, WA: Pacific Northwest National Laboratory.https://doi.org/10.2172/882976

Trenberth, K. E., Dai, A., van der Schrier, G., Jones, P. D., Barichivich, J., Briffa, K. R., & Sheffield, J. (2013). Global warming and changes in drought. *Nature Climate Change*, *4*(1), 17–22. https://doi.org/10.1038/nclimate2067

Vickers, D., & Mahrt, L. (1997). Quality control and flux sampling problems for tower and aircraft data. *Journal of Atmospheric and Oceanic Technology*, *14*(3), 512–526. https://doi.org/10.1175/1520-0426(1997)014<0512:QCAFSP>2.0.CO;2

Webb, E. K., Pearman, G. I., & Leuning, R. (1980). Correction of flux measurements for density effects due to heat and water vapour transfer. *Quarterly Journal of the Royal Meteorological Society*, *106*(447), 85–100. https://doi.org/10.1002/qj.49710644707

Wilczak, J. M., Oncley, S. P., & Stage, S. A. (2001). Sonic anemometer tilt correction algorithms. *Boundary-Layer Meteorology*, *99*(1), 127–150. https://doi.org/10.1023/A:1018966204465

Williams, M. D., Rockhold, M. L., Thorne, P. D., & Chen, Y. (2008). Three-dimensional groundwater models of the 300 area at the Hanford Site, Washington State, Rep. PNNL-17708 (No. PNNL-17708). Richland, WA: Pacific Northwest National Laboratory. https://doi.org/10.2172/969184

Wutzler, T., Lucas-Moffat, A., Migliavacca, M., Knauer, J., Sickel, K., Šigut, L., et al. (2018). Basic and extensible post-processing of eddy covariance flux data with REddyProc. *Biogeosciences Discussions*, 1–39. https://doi.org/10.5194/bg-2018-56